Electronic Supplementary Material (ESI) for Nanoscale.
This journal is © The Royal Society of Chemistry 2023

Supporting Information for:

Influence of Surface and Intermolecular Interactions on the Properties of Supported Polyoxometalates

Oliva M. Primera-Pedrozo,[1] Shuai Tan,[1] Difan Zhang,[1] Brian T. O'Callahan,[2] Wenjin Cao,[1] Eric T. Baxter,[1] Xue-Bin Wang,[1] Patrick Z. El-Khoury,[1] Venkateshkumar Prabhakaran,[1] Vassiliki-Alexandra Glezakou,[3] and Grant E. Johnson[1]*

[1]Pacific Northwest National Laboratory, Physical Sciences Division, P.O. Box 999, MSIN J7-10, Richland, Washington 99352, United States

[2]Pacific Northwest National Laboratory, Earth and Biological Sciences Division, P.O. Box 999, MSIN K8-88, Richland, Washington 99352, United States

[3]Oak Ridge National Laboratory, 1 Bethel Valley Road, Oak Ridge, Tennessee 37830, United States

*Email: grant.johnson@pnnl.gov

EXPERIMENTAL AND THEORETICAL METHODS

Chemicals

Sodium phosphotungstate hydrate ($Na_3PO_4 \cdot 12WO_3 \cdot xH_2O$, CAS: 312696-30-3, 99%), sodium metavanadate ($NaVO_3$, CAS: 13718-26-8, ≥98%), 1-dodecanethiol (≥98%), 1H,1H,2H,2H-perfluorodecanethiol (97%), and 11-mercaptoundecanoic acid (98%) were all purchased from Sigma-Aldrich and used for the preparation of VPOM solutions and HSAM, FSAM, and COOH-SAM surfaces, respectively. All $VPOM^{4-}$ syntheses were performed using deionized water (~18.1 MΩ) obtained from an ion exchange system, [U.S. Filter, (Snellville, GA)].

Synthesis of Vanadium-Doped Tungsten Keggin Polyoxometalates

Throughout this contribution, we use the abbreviated notation $VPOM^{4-}$ to indicate $PVW_{11}O_{40}^{4-}$ and $WPOM^{3-}$ to specify $PW_{12}O_{40}^{3-}$, respectively. $VPOM^{4-}$ were prepared in aqueous solution using a one-pot synthesis procedure described in the literature with modifications.[1-3] In a representative synthesis, 15 mL of deionized water at ~pH 7 was heated to ~70°C for ~10 min. An 11:1 molar ratio of $Na_3PO_4 \cdot 12WO_3 \cdot xH_2O$:$NaVO_3$ salts was added to the water and stirred vigorously for 30 min whereupon the color of the solution visually changed from clear to dark orange. The final stock solution of $VPOM^{4-}$, which had a concentration of ~0.1 M, was cooled to room temperature. Solutions for analysis by electrospray ionization mass spectrometry (ESI-MS) were prepared by diluting the ~0.1 M stock solution to ~100 μM in methanol. ESI-MS characterization of the $VPOM^{4-}$ solutions was performed using an Orbitrap Elite Mass Spectrometer (M/ΔM = 60,000 mass resolution, Thermo Fisher Scientific, San Jose, CA) operated in the negative ion mode. The mass spectrometer conditions were as follows: capillary temperature, 325°C; spray voltage, 5 kV; capillary voltage, 4 V; tube lens, 55 V; s-lens radiofrequency (RF) level; RF amplitude, 400 V, and a mass range of m/z = 75 – 2000. The diluted samples of $VPOM^{4-}$ were infused into the instrument using a syringe pump through custom-assembled tubing (fused silica Molex capillaries, 75 μm internal diameter, 360 μm outer diameter) at a flow rate of 60 μL/hr.

Preparation of Self-Assembled Monolayers on Gold

All of the self-assembled monolayers (SAMs) on gold were prepared on 10 × 10 mm polycrystalline gold surfaces with a 50 Å thick titanium adhesion layer and a 1000 Å thick gold layer on an underlying silicon wafer [Platypus Technologies, (Madison, WI)]. The as received gold surfaces were cleaned by sonication in ethanol for 10 min, dried using a stream of nitrogen gas, and placed in an ultraviolet/ozone cleaner for 15 min before being immersed in freshly prepared 1 mM ethanolic solutions of the SAMs. The HSAM,[4] FSAM,[5] and COOH-SAM[6] on gold surfaces were prepared following established procedures reported previously in the literature.[7] All SAMs were prepared by immersing the recently cleaned gold coated surfaces in 1 mM ethanolic solutions of the thiols at room temperature for at least 24 hours in the dark.[8] The SAM substrates were then removed from solution, rinsed with ethanol, and sonicated in ethanol for 5 min to remove any loosely bound secondary layers of thiols. The SAM surfaces were rinsed with ethanol a final time, dried under nitrogen, and introduced into vacuum on a sample holder for ISL experiments.

Ion Soft Landing

Ion soft landing (ISL) experiments were performed using a specialized high-flux ion deposition apparatus designed and constructed at Pacific Northwest National Laboratory and described in detail in previous publications.[8-10] Gas-phase POM anions were produced using electrospray ionization (ESI)[11] and introduced into the vacuum system through a heated stainless steel inlet capillary maintained at a temperature of ~120°C. Desolvated POM anions were transferred through a series of two high-transmission electrodynamic ion funnels[12] and radially focused and thermalized by collisions with the background gas in a radiofrequency (RF)-only collision quadrupole ion guide maintained at a pressure of ~2 x 10^{-2} Torr (mostly N_2). A mass resolving quadrupole filter (Extrel, Pittsburgh, PA), maintained at a pressure of ~1 x 10^{-5} Torr, was used to select $VPOM^{4-}$ by mass-to-charge ratio (*m/z*) for deposition. Mass-selected anions exiting the resolving quadrupole were recollimated in a second collision quadrupole ion guide, steered 90° with a quadrupole bender, and focused using a series of einzel lenses to produce a circular deposition area ~3 mm in diameter on the SAM surfaces. The ion current at the surface was measured throughout the

deposition with a floatable picoammeter (Model 9103, RBD Instruments, Bend, OR) and used to determine and control the surface coverage of $VPOM^{4-}$. The kinetic energy of the POM anions arriving at the substrates was maintained in a range of 10 – 15 eV per charge by applying a repulsive negative potential to the surfaces through the floatable picoammeter.

Negative Ion Photoelectron Spectroscopy

Negative ion photoelectron spectroscopy (NIPE) spectra were obtained in the gas phase using a custom-built magnetic bottle time-of-flight (TOF) photoelectron spectrometer combined with an electrospray ionization (ESI) source and a temperature-controlled cryogenic ion trap.[13] The quadruply-charged $VPOM^{4-}$ anions were generated by electrospraying a ~0.1 mM acetonitrile solution of $[Bu_4N]_4[PVW_{11}O_{40}]$ in the negative ion mode. The resulting anions were transported by a RF-only quadrupole ion guide and detected by a mass resolving quadruple filter and detector to optimize the ESI conditions to ensure sufficiently stable and intense ion beams for reliable spectroscopic measurements. The anions were then directed by a 90˚ quadrupole bender into the cryogenic 3-dimensional ion trap where they were accumulated for 20 – 100 ms and cooled by collisions with cold He buffer gas to the desired temperature of T = 20K. The cooled ions were then pulsed into the extraction zone of the TOF mass spectrometer for mass analysis at a repetition rate of 10 Hz. The anions of interest were mass-selected and decelerated before being photodetached by a 157 nm (7.866 eV, Lambda Physik CompexPro F_2) or 193 nm (6.424 eV, GAM EX100F ArF) laser beam in the interaction zone of the magnetic-bottle photoelectron analyzer. The probe lasers were operated at a 20 Hz repetition rate with the anion beam shut off on alternating laser shots to afford real-time shot-to-shot background subtraction. The resulting photoelectrons were collected at nearly 100% efficiency in the magnetic-bottle and analyzed with a 5.2 m long electron flight tube. Recorded flight times were converted into calibrated kinetic energies using the known photoelectron spectrum of $I^-/OsCl_6^{2-}$.[14, 15] Electron binding energies (EBEs) were obtained by subtracting the measured electron kinetic energies from the detachment photon energy with an energy resolution ($\Delta E/E$) of about 2% (*i.e.,* ~20 meV for 1 eV kinetic energy electrons).

Atomic Force Microscopy

Atomic force microscopy (AFM) topographic and multimodal chemical imaging methods were used to identify and characterize well-defined $VPOM^{4-}$ and their assemblies soft landed on different SAM surfaces. To map the localized work function (WF) of the SAM substrates before and after soft landing of $VPOM^{4-}$, scanning Kelvin probe microscopy (KPFM) measurements were conducted using a commercially available AFM (NX10, Park Systems, Inc). A NSC14/Cr-Au (Mikromasch) probe, with a WF of 4.985 eV derived from calibration with highly oriented pyrolytic graphite (HOPG, 4.650 eV), was driven at a frequency of 160 kHz with a peak-to-peak amplitude of 20 nm. A lock-in amplifier was applied with a 2 V drive at 17 kHz frequency to differentiate the electrostatic from the Van der Waals forces between the tip and sample. In this manner, the WF and topography of $WPOM^{3-}$ and $VPOM^{4-}$ soft landed on different SAM surfaces were mapped simultaneously.

Infrared Reflection Absorption Spectroscopy of Soft Landed Polyoxometalates

Infrared reflection absorption spectroscopy (IRRAS) was performed on the soft landed POMs *ex situ* using a Vertex 70 Fourier transform infrared (FTIR) spectrometer (Bruker Optics, Billerica, MA) equipped with a liquid-nitrogen-cooled mercury-cadmium-telluride (MCT) detector. IR spectra were obtained by acquiring 1500 scans (~6 min) with 2 cm^{-1} resolution over a wavenumber range of 800 – 4000 cm^{-1}. The IR beam path was continuously purged with N_2 gas during the spectroscopy experiments to minimize atmospheric contributions to the signal. Plots of the experimental IRRAS data were smoothed and baseline-corrected in interactive mode using the OPUS software.

Scattering-Type Scanning Near-Field Optical Microscopy

Scattering-type scanning near-field optical microscopy (s-SNOM) was performed to analyze how POM-POM and POM-surface interactions influence the vibrational modes of $VPOM^{4-}$ as a function of surface coverage. Briefly, the output of a broadband, tunable laser (Carmina, Applied Physics Instruments) was focused by a parabolic mirror [numerical aperture (NA) = 0.4] onto the apex of a gold-coated AFM tip

(AFM+, Bruker) operating in tapping mode. The tip-scattered light, which reflects the local optical properties of the sample surface with a spatial resolution of tens of nanometers, was collected by the parabolic mirror, combined with light from a reference arm, and sent to an IR detector. Far-field background was removed by demodulating the detector signal at the second harmonic of the tip tapping frequency. Spectra were obtained interferometrically using an asymmetric Michelson geometry.

Tip Enhanced Raman Spectroscopy

Nanoholes were prepared by pulse force nanolithography on template-stripped gold films (Platypus Technologies, AU.1000.SWTSG) of 100 nm thickness using arrow tips (Nanoworld, ARROW-NCR) and single crystal diamond tips (Artech Carbon OÜ, D300).[16] These nanoholes were separated by 2 μm to ensure that the focused microscopic light source only irradiated a single nanostructure. High spatial resolution AFM maps were recorded using super sharp AFM tips (Nanosensors, SSS-NCHR). Gold coated 100 nm thick AFM tips (Nanosensors, ATEC-NC) were used to record tip enhanced Raman (TER) spectra following 633 nm (0.3 mW) irradiation. Signals were time-integrated for 0.1 – 0.25 sec, depending on signal levels. The TERS experimental set-up is described in detail in previous works.[17]

Theoretical Calculations

Density functional theory (DFT) calculations were carried out using ORCA[18] to obtain atomistic-level information on $WPOM^{3-}$ and $VPOM^{4-}$. Initial POM structures were obtained from the literature[19] and used as starting points for geometry optimization.[20] All geometry optimization, electronic structure evaluation, and IR/Raman spectra calculations were performed using the hybrid B3LYP functional.[21] The Stuttgart 14-valence electron pseudo-potentials and basis sets for vanadium and tungsten,[22] and the def2-TZVP basis sets for oxygen and phosphorus were used. This protocol was employed in previous calculations and shown to produce reasonable results.[23] The structural minima were confirmed by normal mode frequency analysis. IR and Raman spectra of the geometrically optimized structures were visualized using the Avogadro software to assign the vibrational peaks. The electrostatic potential (ESP) and electron spin density (ESD)

maps were generated using Multiwfn.[24] The electron vertical detachment energies (VDEs) were calculated as the energy differences between POM^{n-} and $POM^{(n+1)-}$, both at the optimized geometry of $POM^{(n+1)-}$. The electron adiabatic detachment energies (ADEs) were calculated as the energy difference between the POM^{n-} and $POM^{(n+1)-}$ at each optimized geometry including zero-point vibration energy corrections.

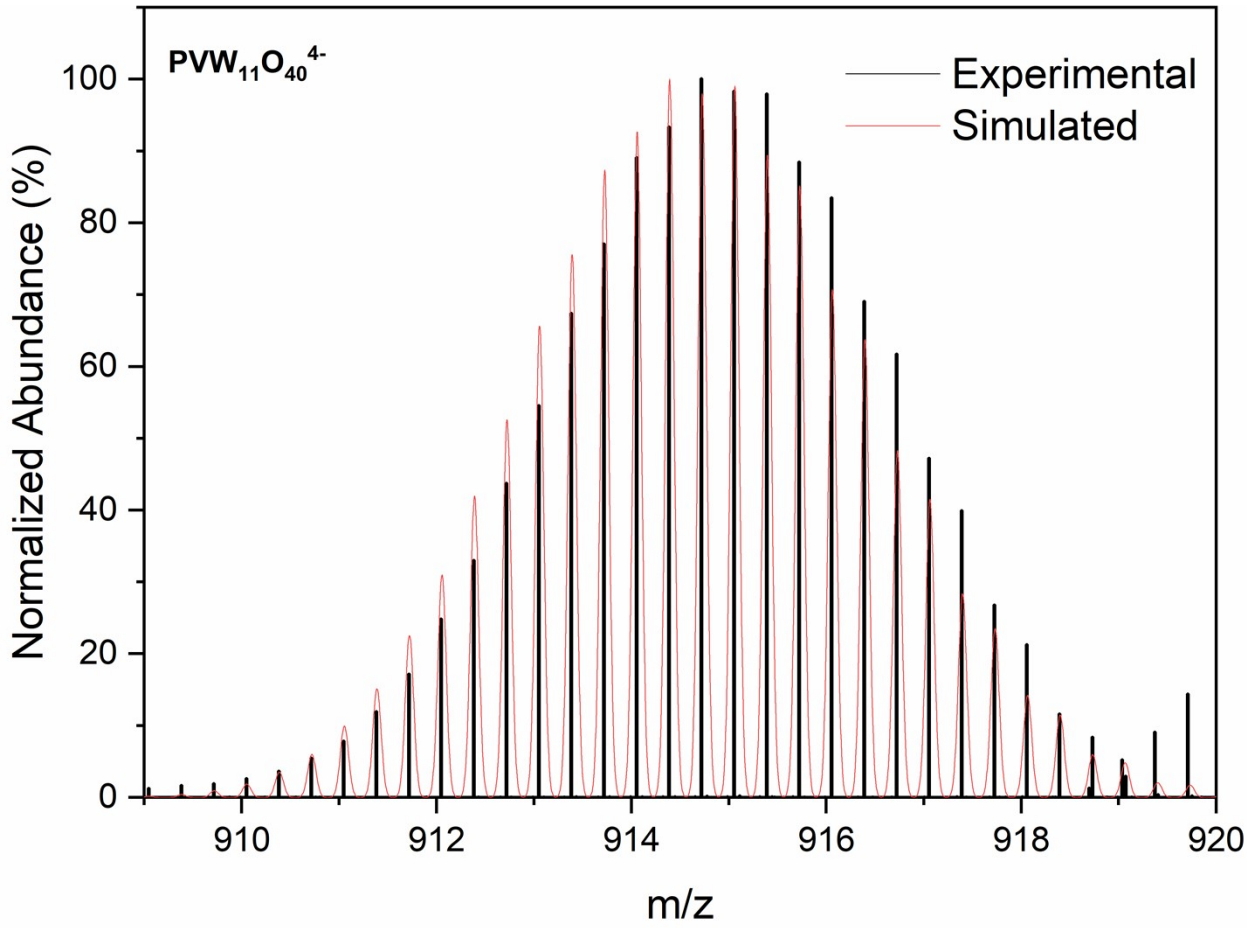

Figure S1. Comparison between the experimentally measured mass spectrum (M/ΔM = 60,000 mass resolution) and simulated spectrum generated using the mMass software of a mixed-addenda POM prepared with molar ratio of 11:1 of $Na_3PO_4 \cdot 12WO_3 \cdot xH_2O$ and $NaVO_3$ at pH 7, showing the presence of the V-doped POM anion $PVW_{11}O_{40}^{4-}$ ($VPOM^{4-}$).

Table S1. Comparison between the experimentally measured mass spectrum (M/ΔM = 60,000 mass resolution) and the simulated spectrum.

$PVW_{11}O_{40}^{4-}$				
Calculated (mMass)		Measured (100 K)		
m/z	Intensity	m/z	Intensity	Δ m/z
682.7896702	3.517086176	682.85823	3.457021343	-0.069
683.0401084	6.007224692	683.04216	1.748995279	-0.002
683.2905227	9.956676873	683.29321	1.754848024	-0.003
683.5409789	15.13438403	683.54286	6.78820867	-0.002
683.7914037	22.53295747	683.79363	21.94389169	-0.002
684.0418461	30.96854473	684.04411	26.42709431	-0.002
684.2922658	41.98201976	684.2945	35.45105154	-0.002
684.542652	52.64718816	684.54471	49.82149128	-0.002
684.7929391	65.65469052	684.79514	64.79476374	-0.002
685.0432422	75.60678646	685.04559	84.06297554	-0.002
685.2935202	87.39933601	685.29592	95.31292676	-0.002
685.5438263	92.76510475	685.54635	91.93686839	-0.003
685.7941112	100	685.79672	100	-0.003
686.0444996	97.95640276	686.04707	95.22611105	-0.003
686.2949155	98.97920586	686.29764	89.8669476	-0.003
686.5453848	89.39171658	686.54788	95.54118382	-0.002
686.7958011	85.08279175	686.79815	90.85020875	-0.002
687.0462984	70.65181094	687.04865	71.35081353	-0.002
687.2966994	63.7484581	687.29891	62.56096609	-0.002
687.5471946	48.29761645	687.54951	44.98712396	-0.002
687.7975631	41.55623382	687.79965	35.65687307	-0.002
688.0479175	28.38429623	688.05013	26.2437083	-0.002
688.2981706	23.51460036	688.3003	19.95493386	-0.002
688.5485282	14.21383199	688.550632	9.53509696	-0.002
688.7987667	11.50181619	688.801627	9.659955519	-0.003
689.0491556	5.976903598	689.0665	9.494127746	-0.017
689.2994286	4.829749772	689.30027	8.489406532	-0.001
689.5500422	2.062077442	689.56742	4.069608646	-0.017
689.8003379	1.72183636	689.81712	4.545631901	-0.017
690.0510197	0.562071693	690.067981	1.374734108	-0.017
690.3012815	0.511819962	690.316637	2.634173169	-0.015
690.5520181	0.113611999	690.561813	6.637843699	-0.010
690.8022238	0.1225209	690.812294	4.501304479	-0.010

Supporting References

1 K. D. D. Gunaratne, V. Prabhakaran, G. E. Johnson, J. Laskin, Gas-Phase Fragmentation Pathways of Mixed Addenda Keggin Anions: $PMo_{12-n}W_nO_{40}^{3-}$ (n=0-12), *J. Am. Soc. Mass. Spectrom.*, 2015, **26**, 1027-1035.

2 J. J. Altenau, M. T. Pope, R. A. Prados, H. So, Models for Heteropoly Blues - Degrees of Valence Trapping in Vanadium(IV)-Substituted and Molybdenum(V)-Substituted Keggin Anions, *Inorg. Chem.*, 1975, **14**, 417-421.

3 V. Prabhakaran *et al.*, Controlling the Activity and Stability of Electrochemical Interfaces Using Atom-by-Atom Metal Substitution of Redox Species, *ACS Nano*, 2019, **13**, 458-466.

4 H. Ron, S. Matlis, I. Rubinstein, Self-Assembled Monolayers on Oxidized Metals. 2. Gold Surface Oxidative Pretreatment, Monolayer Properties, and Depression Formation, *Langmuir*, 1998, **14**, 1116-1121.

5 H. Fukushima *et al.*, Microstructure, Wettability, and Thermal Stability of Semifluorinated Self-Assembled Monolayers (SAMs) on Gold, *J. Phys. Chem. B*, 2000, **104**, 7417-7423.

6 H. Wang, S. Chen, L. Li, S. Jiang, Improved Method for the Preparation of Carboxylic Acid and Amine Terminated Self-Assembled Monolayers of Alkanethiolates, *Langmuir*, 2005, **21**, 2633-2636.

7 S. Farhadi, M. Taherimehr, Vanadium-Substituted Tungstophosphoric Acid ($H_5PV_2W_{10}O_{40}$): A Green and Reusable Catalyst for Highly Efficient Acetylation of Alcohols and Phenols under Solvent-free Conditions, *Acta. Chim. Slov.*, 2008, **55**, 637-643.

8 K. D. D. Gunaratne *et al.*, Controlling the Charge State and Redox Properties of Supported Polyoxometalates via Soft Landing of Mass-Selected Ions, *J. Phys. Chem. C*, 2014, **118**, 27611-27622.

9 G. E. Johnson, M. Lysonski, J. Laskin, In Situ Reactivity and TOF-SIMS Analysis of Surfaces Prepared by Soft and Reactive Landing of Mass-Selected Ions, *Anal. Chem.*, 2010, **82**, 5718-5727.

10 K. D. D. Gunaratne *et al.*, Design and performance of a high-flux electrospray ionization source for ion soft landing, *Analyst*, 2015, **140**, 2957-2963.

11 J. B. Fenn, M. Mann, C. K. Meng, S. F. Wong, C. M. Whitehouse, Electrospray Ionization for Mass-Spectrometry of Large Biomolecules, *Science*, 1989, **246**, 64-71.

12 R. T. Kelly, A. V. Tolmachev, J. S. Page, K. Q. Tang, R. D. Smith, The Ion Funnel: Theory, Implementations, and Applications, *Mass. Spectrom. Rev.*, 2010, **29**, 294-312.

13 Q. Yuan, W. Cao, X.-B. Wang, Cryogenic and Temperature-Dependent Photoelectron Spectroscopy of Metal Complexes, *Int. Rev. Phys. Chem.*, 2020, **39**, 83-108.

14 D. Hanstorp, M. Gustafsson, Determination of the Electron Affinity of Iodine, *J Phys. B: At., Mol. Opt. Phys.*, 1992, **25**, 1773.

15 X.-B. Wang, L.-S. Wang, Photodetachment of Free Hexahalogenometallate Doubly Charged Anions in the Gas Phase: $[ML_6]^{2-}$, (M=Re, Os, Ir, Pt; L=Cl and Br), *J. Chem. Phys.*, 1999, **111**, 4497-4509.

16 A. Bhattarai *et al.*, Tip-Enhanced Raman Scattering from Nanopatterned Graphene and Graphene Oxide, *Nano Lett.*, 2018, **18**, 4029-4033.

17 A. Bhattarai *et al.*, Tip-Enhanced Raman Nanospectroscopy of Smooth Spherical Gold Nanoparticles, *J. Phys. Chem. Lett.*, 2020, **11**, 1795-1801.

18 F. Neese, F. Wennmohs, U. Becker, C. Riplinger, The ORCA quantum chemistry program package, *J. Chem. Phys.*, 2020, **152**, 224108.

19 M. J. Watras, A. V. Teplyakov, Infrared and computational investigation of vanadium-substituted Keggin $[PV_nW_{12-n}O_{40}]^{n+3}$ polyoxometallic anions, *J. Phys. Chem. B*, 2005, **109**, 8928-8934.

20 J. Zhang, V. A. Glezakou, R. Rousseau, M. T. Nguyen, NWPEsSe: An Adaptive-Learning Global Optimization Algorithm for Nanosized Cluster Systems, *J. Chem. Theory. Comput.*, 2020, **16**, 3947-3958.
21 A. D. Becke, Density-Functional Thermochemistry .1. The Effect of the Exchange-Only Gradient Correction, *J. Chem. Phys.*, 1992, **96**, 2155-2160.
22 D. Andrae, U. Haussermann, M. Dolg, H. Stoll, H. Preuss, Energy-Adjusted Ab initio Pseudopotentials for the 2nd and 3rd Row Transition-Elements, *Theor. Chim. Acta.*, 1990, **77**, 123-141.
23 T. Waters *et al.*, Photoelectron Spectroscopy of free multiply charged keggin anions alpha-$[PM_{12}O_{40}]^{3-}$ (M = Mo, W) in the gas phase, *J. Phys. Chem. A*, 2006, **110**, 10737-10741.
24 T. Lu, F. W. Chen, Multiwfn: A multifunctional wavefunction analyzer, *J. Comput. Chem.*, 2012, **33**, 580-592.